Structure
Article

# Structural Investigation of Rimantadine Inhibition of the AM2-BM2 Chimera Channel of Influenza Viruses

Rafal M. Pielak,[1] Kirill Oxenoid,[1] and James J. Chou[1,*]
[1]Jack and Eileen Connors Structural Biology Laboratory, Department of Biological Chemistry and Molecular Pharmacology, Harvard Medical School, Boston, MA 02115, USA
*Correspondence: chou@cmcd.hms.harvard.edu
DOI 10.1016/j.str.2011.09.003

## SUMMARY

**The M2 channel of influenza A is a target of the adamantane family antiviral drugs. Two different drug-binding sites have been reported: one inside the pore, and the other is a lipid-facing pocket. A previous study showed that a chimera of M2 variants from influenza A and B that contains only the pore-binding site is sensitive to amantadine inhibition, suggesting that the primary site of inhibition is inside the pore. To obtain atomic details of channel-drug interaction, we determined the structures of the chimeric channel with and without rimantadine. Inside the channel and near the N-terminal end, methyl groups of Val27 and Ala30 from four subunits form a hydrophobic pocket around the adamantane, and the drug amino group appears to be in polar contact with the backbone oxygen of Ala30. The structures also reveal differences between the drug-bound and -unbound states of the channel that can explain drug resistance.**

## INTRODUCTION

The M2 proteins of influenza A and B virus, AM2 and BM2, respectively, are transmembrane (TM) proteins that tetramerize in the viral membrane to form channel structures that selectively transport protons across the membrane (Mould et al., 2003; Paterson et al., 2003; Pinto et al., 1992; Sugrue and Hay, 1991). The role of proton conduction by M2 is believed to equilibrate pH across the viral membrane during cell entry and across the trans-Golgi membrane of infected cells during viral maturation (Hay et al., 1985; Helenius, 1992). Proton conductance depends on the pH and pH difference across the membrane, and the channel is essentially in a closed conformation at pH >7.5 (Pielak and Chou, 2010a; Wang et al., 1995). The transport activity of AM2, but not BM2, can be blocked by the adamantane family antiviral compounds, of which the amantadine and rimantadine were the first effective drugs licensed for influenza treatment (Davies et al., 1964). The majority of the circulating virus strains are now resistant to these drugs (Bright et al., 2006), and at least six single mutations in the AM2 TM region have been reported that confer drug resistance. Therefore, it is of interest to obtain a precise picture of drug binding for understanding the mechanism of drug resistance and for developing a next-generation antiflu compound that targets M2.

Recent structural characterizations of the channel domain of AM2 have included solution NMR structures of the wild-type AM2 (Schnell and Chou, 2008) and the drug-resistant mutants S31N (Pielak et al., 2009) and V27A (Pielak and Chou, 2010b), crystal structures of AM2 at different pH values (Khurana et al., 2009; Stouffer et al., 2008), and backbone structures of AM2 derived from solid-state NMR measurements of proteins in lipid bilayers (Cady et al., 2010; Sharma et al., 2010). Moreover, the structure of the BM2 channel has also been determined by solution NMR methods (Wang et al., 2009). These structural models show that a left-handed four-helical bundle forms the channel pore, and that tetramerization of the four TM helices is further stabilized by intermolecular contacts between C-terminal amphipathic helices flanking the TM domain. The packing of Trp41 indole rings creates a channel gate, which closes off the C-terminal end of the pore. The imidazole rings of His37, which are essential in transporting protons, are inside the pore.

Two different drug-binding sites have been reported, leading to proposals for two different mechanisms of drug inhibition. The structure of the TM domain of AM2 (residues 22–46) crystallized in the presence of amantadine showed electron density in the channel pore, near Ser31 (Stouffer et al., 2008), directly blocking the channel passage near the N-terminal end of the pore. However, the position and orientation of amantadine could not be defined unambiguously by the relatively low-resolution data (3.5 Å) because the diameter of the roughly spherical adamantane cage is ~3.5 Å. The solution NMR structure of a longer channel construct (residues 18–60) showed that rimantadine binds near the C-terminal end of the channel to an external site consisting of Trp41, Ile42, and Arg45 from one TM helix and Leu40, Leu43, and Asp44 from the adjacent TM helix (Schnell and Chou, 2008). If this were the site of inhibitory binding, the mechanism would be allosteric: drug binding would stabilize a closed conformation of the channel. Subsequent solid-state NMR measurements using the TM domain reconstituted in lipids confirmed the existence of both binding sites, and reported that the site in the pore has greater affinity for the drug than the external site (Cady et al., 2010).

Independent of the structural studies, a functional experiment using an AM2-BM2 fusion protein provided probably the most convincing resolution to the controversy. In the fusion protein

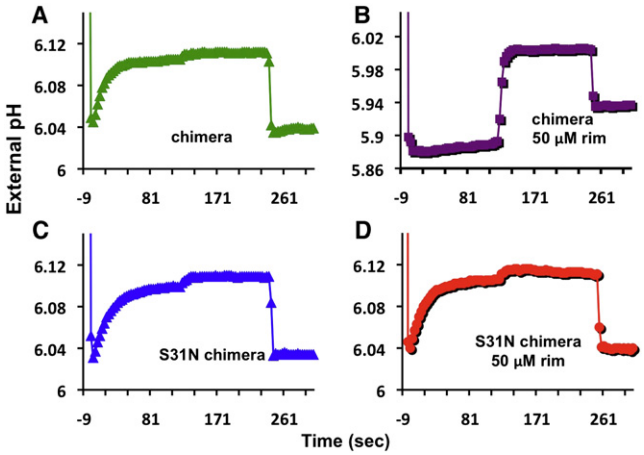


**Figure 1. Functional Investigation of the $(AM2\text{-}BM2)_{TM}$ Channel by the Liposomal Proton Flux Assay**

(A) The conductance of the $(AM2\text{-}BM2)_{TM}$ channel exhibits similar conductance rate (~10 $H^+$/s/channel) as the wild-type AM2 channel (Pielak and Chou, 2010a).

(B) The conductance of $(AM2\text{-}BM2)_{TM}$ was reduced by ~95% by the addition of 50 μM rimantadine (rim).

(C) Introducing the S31N mutation to $(AM2\text{-}BM2)_{TM}$ did not affect its proton conduction rate.

(D) However, the S31N mutation completely abolished inhibition by rimantadine (rim).

the N-terminal half of the channel domain is from AM2 (drug sensitive and contains the pore-binding site), and the C-terminal half is from BM2 (drug insensitive and does not contain the external binding site). It was reported that proton conduction of this AM2-BM2 chimera could still be blocked by amantadine and rimantadine, providing a compelling argument that the functional binding pocket is located in the N-terminal half of the channel pore (Jing et al., 2008; Ohigashi et al., 2009).

Inspired by the above functional experiment, we have carried out a structural investigation of drug binding to the AM2-BM2 fusion protein. We find that a protein construct corresponding to the TM region of the AM2-BM2 chimera, $(AM2\text{-}BM2)_{TM}$, reproduces functional properties unique to the wild-type AM2 channel in a liposomal proton flux assay. The $(AM2\text{-}BM2)_{TM}$ protein reconstituted in detergent micelles can be used to record high-quality NMR spectra, and addition of rimantadine causes large chemical shift perturbations. The high-quality NMR data provide an extensive set of unambiguous structural restraints, which we have used to determine high-resolution structures of the chimeric channel in the drug-bound and -unbound states. Our results show that rimantadine indeed binds inside the pore, supported by specific hydrophobic and polar interactions with the pore-lining residues of the channel, and that drug binding alters the channel conformation.

## RESULTS

### The AM2-BM2 Construct for Characterizing Rimantadine Binding

Both AM2 and BM2 have unstructured N-terminal segments, a channel-forming TM helix, and a relatively long cytoplasmic region (Lamb et al., 1985; Paterson et al., 2003). The residue numbers of the TM helix are 26–46 for AM2 and 5–31 for BM2. There is almost no sequence identity between the two proteins except the conserved histidine (His37 in AM2 and His19 in BM2) and tryptophan (Trp41 in AM2 and Trp23 in BM2) that are necessary for proton selectivity and ion gating of the channels (Mould et al., 2003; Tang et al., 2002; Wang et al., 1995). Whole-cell channel recording experiments showed that replacing residues 1–19 of the full-length BM2 protein, which is insensitive to amantadine, with residues 1–37 of AM2 introduced a hybrid protein sensitive to drug inhibition (Jing et al., 2008; Ohigashi et al., 2009). The result suggests that the primary site of drug action is contained in the half of the TM domain N terminal to the centrally located His37. To characterize drug binding to the AM2-BM2 chimera, we constructed a fusion peptide corresponding to the channel-forming region of the chimera that is amenable to structural studies. This peptide contains residues 18–37 of AM2, followed by residues 20–34 from BM2. In this study we refer to this peptide as $(AM2\text{-}BM2)_{TM}$, and number the residues (18–52) such that they are consistent with the residue numbering for the native AM2 channel.

### Functional Relevance of the $(AM2\text{-}BM2)_{TM}$ Construct

The $(AM2\text{-}BM2)_{TM}$ construct is not a natural sequence, and thus, the relevance of using this peptide for understanding drug inhibition needs to be investigated. The proton conduction and drug inhibition of $(AM2\text{-}BM2)_{TM}$ were tested using a liposomal proton flux assay established earlier (Pielak et al., 2009). In this assay a known quantity of channel protein was reconstituted into liposomes. Proton conduction was initiated by the addition of concentrated acid to the external solution under conditions of rapid solution mixing and then followed as an increase in pH of the external solution as protons move down the pH gradient into the liposomes (Experimental Procedures). This experimental setup mimics what occurs after endocytosis of the virus, as the host cell acidifies the endosomal compartments. Using the liposome assay, we first found that $(AM2\text{-}BM2)_{TM}$ has similar proton conduction properties as the native AM2 and exhibits similar drug sensitivity (Figures 1A and 1B). The chimera and the native AM2 channels both showed approximately 10 $H^+$/s/channel conduction rate, which is ~95% inhibited with 50 μM rimantadine (Figures 1A and 1B) (Pielak et al., 2009). We then used a $(AM2\text{-}BM2)_{TM}$ peptide with the S31N mutation, which is a prevalent drug-resistance mutation that accounts for the majority of all resistant viruses (Bright et al., 2006; Hay et al., 1985), to test whether the mutant $(AM2\text{-}BM2)_{TM}$ also acquires drug resistance. Indeed, the proton conductance of the S31N chimera was not affected by 50 μM rimantadine (Figures 1C and 1D), similar to what we found for the S31N mutant of AM2 in the same assay (Pielak et al., 2009). These results indicate that channels formed by the $(AM2\text{-}BM2)_{TM}$ peptide in liposomes are almost identical to native AM2 in proton conduction, rimantadine inhibition, and rimantadine resistance.

### Functional Relevance of the $(AM2\text{-}BM2)_{TM}$ NMR System

For structural characterization of the chimera channel, we reconstituted the $(AM2\text{-}BM2)_{TM}$ peptide in dihexanoyl-phosphatidylcholine (DHPC) detergent micelles and found that the protein runs on SDS-PAGE as a stable tetramer (see Figure S1 available

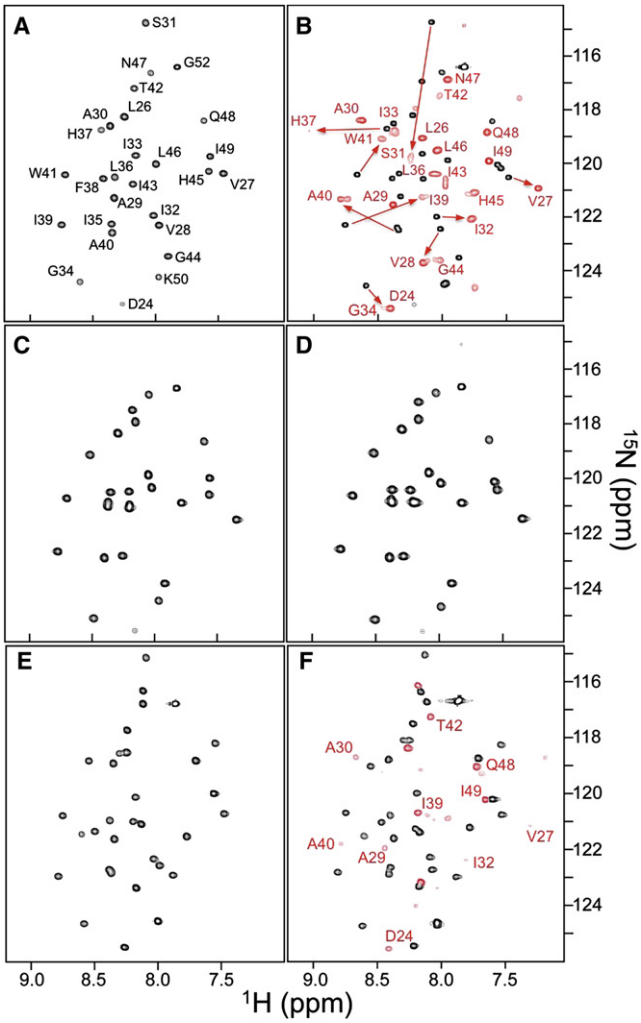


**Figure 2. Functional Investigation of the $(AM2\text{-}BM2)_{TM}$ Channel by NMR**

The $^{1}H$-$^{15}N$ TROSY-HSQC spectra of the $(AM2\text{-}BM2)_{TM}$ (1.4 mM monomer) reconstituted in DHPC are as follows: (A) at pH 7.5; (B) at pH 7.5 with 50 mM rimantadine; (C) with the S31N mutation at pH 7.5; (D) same as in (C) but with 50 mM rimantadine; (E) at pH 6.1; and (F) at pH 6.1 with 100 mM rimantadine. The red peaks correspond to resonances that have emerged upon addition of rimantadine. Please also see Figure S1–S4.

online). The reconstituted tetramer generated very similar $^{1}H$-$^{15}N$ TROSY-HSQC spectra in DHPC (see Experimental Procedures for the full name) micelles and DMPC/DHPC bicelles (q = 0.3) (Figure S2), suggesting that the overall conformation of the protein is essentially the same in detergent as in a lipid environment. The NMR spectra also reflect partial structural similarities between the chimera and the native AM2 and BM2 channels because chemical shifts of the chimera residues that come from the AM2 sequence (18–36) are similar to the corresponding chemical shifts from AM2, and the same is true for those that come from the BM2 sequence (38–52) (Figure S3).

We then tested whether the $(AM2\text{-}BM2)_{TM}$ tetramer exhibits the functional properties of the native AM2 channel under the NMR sample conditions. Upon addition of 50 mM rimantadine to the $(AM2\text{-}BM2)_{TM}$ sample at pH 7.5, a new set of peaks emerged in the TROSY-HSQC spectrum (Figures 2A and 2B). The peaks corresponding to the drug-bound state have very different chemical shifts for almost all residues (the largest changes are around Ser31, ~5 ppm in $^{15}N$ and ~0.16 ppm in $^{1}H$; and His37, ~0.1 ppm in $^{15}N$ and ~0.6 ppm in $^{1}H$) (Figure 2B; Figure S4). This result suggests that the drug binds specifically to the chimeric channel in detergent micelles and that drug binding may have induced substantial conformational change. We did not detect spectral changes for the chimera with the S31N mutation when adding the same amount of the drug to the sample (Figures 2C and 2D), indicating that the chemical shift perturbation in Figure 2B is specific to drug binding and that the NMR system developed for the chimera is suitable for investigating the mechanism of drug binding of the native AM2 channel.

At pH 7.5, the channel is essentially in a closed state (Pielak and Chou, 2010a; Wang et al., 1995). We also investigated whether the drug binds to the open state of the chimeric channel in a more acidic buffer. At pH 6.1, the TROSY-HSQC spectrum of $(AM2\text{-}BM2)_{TM}$ in DHPC micelles (Figure 2E) is significantly different from that at pH 7.5 (Figure 2A). Addition of rimantadine also generates a new set of peaks (Figure 2F) that have similar chemical shifts as those of the drug-bound closed state. At 50 mM rimantadine and pH 6.1, the peaks corresponding to the drug-bound population are barely visible; even at 100 mM, they are ~5-fold less intense than those at pH 7.5. The results suggest that the drug also binds to the open state, but with much lower affinity.

## Location of the Drug-Binding Site in the Chimera Channel

To determine the precise location of drug binding, we made $(AM2\text{-}BM2)_{TM}$ peptide that is $^{15}N$-labeled and 99.9% deuterated at the nonlabile sites so that nuclear Overhauser enhancement (NOE) between the protein backbone amide protons and drug protons could be measured unambiguously. In the presence of 50 mM rimantadine, about 60% of the chimeric channels were drug bound and 40% unbound, as judged by the relative intensities of the NMR peaks. In this case the NMR peaks of the population not bound with drug served as an excellent internal-negative control for measuring protein-drug NOE. We recorded a 3D $^{15}N$-edited NOESY spectrum with 250 ms NOE mixing and found that the amide peaks of Ala30, Ser31, and Ile32 of the drug-bound population showed intense NOE cross-peaks to the adamantane $CH_2$ and CH protons, whereas the peaks of the unbound population did not (Figure 3, left panel). There was also an NOE cross-peak between the amide of Gly17 and the terminal methyl group (1.2 ppm) of rimantadine. Independently of the $^{15}N$-edited NOESY, we recorded a 3D $^{13}C$-edited NOESY (150 ms NOE mixing) using a uniformly $^{15}N$- and $^{13}C$-labeled and nondeuterated protein for identifying NOE between the protein methyl groups and the drug. In this spectrum we unambiguously identified strong NOE cross-peak between the Val27 $C^{\gamma 1}H_3$ group and the adamantane $CH_2$ group of rimantadine (Figure 3, right panel). These NOE data indicate that the drug binds inside the chimera channel near residue positions 27–31.

## Solution Structures of the Chimera Channel with and without Rimantadine

Using the NMR methods established previously for oligomeric, channel-like proteins (Oxenoid and Chou, 2005; Schnell and

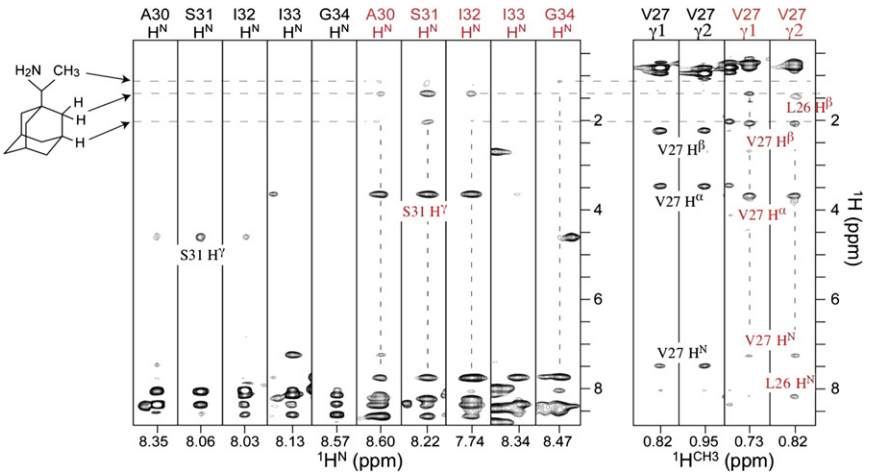


**Figure 3. Selected Regions of NOESY Spectra for Identifying Protein-Drug NOEs**

Left panel shows strips from the 3D $^{15}$N-edited NOESY-tr-HSQC spectrum recorded using the $^{15}$N-, $^{2}$H-labeled chimera in the presence of 50 mM rimantadine.

Right panel illustrates strips from the 3D $^{13}$C-edited NOESY-HSQC spectrum recorded using the $^{15}$N-, $^{13}$C-labled chimera in the presence of 50 mM rimantadine. The resonances of the drug-bound state are labeled in red.

Chou, 2008), we determined the high-resolution structures of the $(AM2\text{-}BM2)_{TM}$ tetramer at pH 7.5 in the presence and absence of rimantadine. Both structures were determined with an extensive set of experimental restraints including intramolecular and intermolecular distances derived from NOE, dihedral angles from chemical shifts, and backbone bond orientations from residual dipolar couplings (RDCs) (Table 1). For the drug-bound structure the restraints also include 16 experimental inter-hydrogen distances between the $(AM2\text{-}BM2)_{TM}$ tetramer and rimantadine. In both cases (drug-bound and -unbound), the structural restraints were used to generate an ensemble of 15 low-energy structures with rmsd of all heavy atoms smaller than 1 Å (Figure 4A and Table 1).

In the absence of rimantadine, the $(AM2\text{-}BM2)_{TM}$ tetramer is a left-handed four-helical bundle that spans about 33 Å in detergent micelles (Figure 4B, left panel). The individual subunits are α helical from residues 26 to 49, but the TM helices show a bend (~17°) near His37. The AM2 and BM2 sequences fuse at His37, and the helical bending may be necessary to satisfy the different helix-helix packing angles in the AM2 and BM2 channel assemblies (−21° in AM2; Schnell and Chou [2008]; and −37° in BM2; Wang et al. [2009]). We also found that the AM2 and BM2 regions of the chimera are structurally very similar to the corresponding regions in the native AM2 and BM2 channels (Figure 4B, right panel). A ring of methyl groups from Val27 constricts the N-terminal end of the channel. The imidazoles of His37 and indoles of Trp41 are both pore lining; their packing closes off the C-terminal end of the channel. The orientations of the Trp41 indoles are more similar to those in the native BM2 channel; they are roughly perpendicular to the channel axis.

The structure of the chimera in complex with rimantadine shows that the drug binds inside the channel, forming numerous contacts with the side chains of Val27 and Ala30. Although the overall structures of the drug-bound and -unbound states of the chimera appear to be very similar, overlay of the two structures reveals substantial differences for the region of the channel in which the drug binds. In particular in the presence of rimantadine, the N-terminal regions (residues 26–34) of the four TM helices are more closely packed than they are in the absence of the drug (Figure 4C, left panel). Furthermore, these regions of the drug-bound TM helices appeared to have been slightly rotated around the individual helical axes relative to the unbound state (Figure 4C, right panel). As a result, the pore-lining methyl groups of Val27 and Ala30 are on average closer to the adamantane cage of the drug.

## Atomic Details of Rimantadine Binding in the Chimera Channel

The structure of the drug-bound channel shows that eight methyl groups of the $(AM2\text{-}BM2)_{TM}$ tetramer (two from each subunit: Val27 $C^{\gamma 1}H_3$ and Ala30 $C^{\beta}H_3$) surround the adamantane cage of rimantadine (Figure 5A). The four $C^{\gamma 1}H_3$ from Val27 are in van der Waals (VDW) contact with $CH_2$ protons on one side of the adamantane, and the four $C^{\beta}H_3$ from Ala30 are at VDW distance from both CH and $CH_2$ protons on all sides of the adamantane (Figure 5A). The eight methyl groups together form a deep internal pocket that completely wraps around the adamantane cage of the drug (Figure 5B). The nitrogen of the rimantadine amino group is on average 2.8 Å from the backbone carbonyl oxygen of Ala30 of one of the four subunits, probably forming a hydrogen bond. The terminal methyl group of the rimantadine is on average roughly in the middle of the pore, facing the open space in the channel around the position of Gly34. Although the rimantadine methyl group does not appear to have extensive hydrophobic interaction with the protein, it is on average at ~4 Å from the Ala30 methyl group and from the α protons of Ser31 and Gly34 of one of the four subunits. The ensemble of structures in Figure 4A also shows that the rimantadine is tilted relative to the channel: its vertical axis is on average ~20° from the C4 symmetry axis of the channel. This tilt angle is consistent with the amantadine tilt in the AM2 channel observed with solid-state NMR spectroscopy (Cady et al., 2010).

The fact that the NMR spectra are symmetric in the presence of this asymmetric interaction indicates fast exchange between the four different asymmetric conformations. Because the largest chemical shift difference between bound and unbound state is ~0.5 ppm at $^{1}$H frequency of 600 Hz, we expect the exchange rate to be much faster than 300 $s^{-1}$.

## DISCUSSION

We have shown that the channel formed by the $(AM2\text{-}BM2)_{TM}$ peptide is a relevant and powerful experimental system for structural investigation of the inhibition of the AM2 channel by

**Table 1. NMR and Refinement Statistics for Protein Structures**

| | $(AM2\text{-}BM2)_{TM}$ (−RIM) | $(AM2\text{-}BM2)_{TM}$ (+RIM) |
|---|---|---|
| NMR Distance and Dihedral Constraints | | |
| Distance constraints | | |
| Total NOE | 149 × 4 | 112 × 4 |
| Intraresidue | 43 × 4 | 23 × 4 |
| Inter-residue | 93 × 4 | 73 × 4 |
| Sequential ($\|i-j\|=1$) | 67 × 4 | 52 × 4 |
| Medium range ($\|i-j\|\leq 4$) | 26 × 4 | 21 × 4 |
| Long range ($\|i-j\|\geq 5$) | 0 | 0 |
| Intermolecular | 13 × 4 | 16 × 4 |
| Hydrogen bonds | 0 | 0 |
| Total dihedral angle restraints | 44 × 4 | 44 × 4 |
| $\phi$ (TALOS) | 22 × 4 | 22 × 4 |
| $\psi$ (TALOS) | 22 × 4 | 22 × 4 |
| $\chi_1$ (J couplings) | 0 | 0 |
| Total RDCs | 26 × 4 | 21 × 4 |
| Backbone NH | 26 × 4 | 21 × 4 |
| Structure Statistics[a] | | |
| Violations (mean ± SD) | | |
| Distance constraints (Å) | 0.064 ± 0.005 | 0.093 ± 0.007 |
| Dihedral angle constraints (°) | 0.838 ± 0.126 | 1.869 ± 0.086 |
| RDC constraints (Hz) | 1.270 ± 0.155 | 1.902 ± 0.084 |
| Deviations from idealized geometry | | |
| Bond lengths (Å) | 0.004 ± 0.000 | 0.005 ± 0.000 |
| Bond angles (°) | 0.543 ± 0.016 | 0.704 ± 0.018 |
| Impropers (°) | 0.407 ± 0.020 | 0.721 ± 0.029 |
| Average pairwise rmsd (Å)[b] | | |
| Heavy | 0.98 | 0.83 |
| Backbone | 0.65 | 0.68 |

[a] Statistics are calculated and averaged over an ensemble of the 15 lowest-energy structures.
[b] The precision of the atomic coordinates is defined as the average rms difference between the 15 final structures and their mean coordinates. The residues 25–49 are included in this calculation.

adamantane family antiviral compounds. The $(AM2\text{-}BM2)_{TM}$ peptide formed channel structures that are similar to the native AM2 in proton conduction, rimantadine inhibition, and resistance to rimantadine. The chimera channels in DHPC micelles can also be used to record high-quality NMR spectra for the closed and open states or in the presence and absence of the drug.

In earlier studies we found that a region of the native AM2 that included residues 18–60 also yielded good NMR spectra when reconstituted in the DHPC micelles, but in that system the channel did not bind rimantadine inside the pore (Schnell and Chou, 2008). Instead, the drug bound at four equivalent pockets at the helix-helix interface near the C-terminal end of the channel, accessible from the lipid bilayer. Trp41, Ile42, and Arg45 from one TM helix and Leu40, Leu43, and Asp44 from the adjacent TM helix create this lipid-facing pocket. We proposed, based on the observation, that the drug binding to the lipid-facing pockets inhibits proton transport allosterically by stabilizing the closed conformation of the channel. However, it was unclear whether the pocket has high enough affinity for the drug to play an important role in inhibition because rimantadine binding at this site only introduced very small changes in the NMR spectrum (Figure S2 in Schnell and Chou, 2008). This is not the case for drug binding inside the channel. Rimantadine binding inside the chimera pore changes the NMR spectrum beyond recognition, which required reassigning the majority of the NMR peaks in the present work (Figure 2B). The large chemical shift changes are consistent with those observed for the native AM2 channels in lipid bilayer using solid-state NMR methods (Andreas et al., 2010; Cady and Hong, 2008). Therefore, our previous NMR system that used residues 18–60 of AM2 reconstituted in DHPC detergent did not support amantadine or rimantadine binding inside the channel, for reasons that remain to be understood. We can only suspect at this point that DHPC somehow interferes with rimantadine binding, possibly by increasing the energy barrier for the drug to enter the channel. Even for the chimeric channel in DHPC micelles, 50 mM rimantadine only yielded ~60% channel occupancy, whereas 50 μM rimantadine applied in the liposome assay achieved 95% inhibition. The large discrepancy is less when considering the effective drug concentration in surfactants because rimantadine partitions strongly in detergents and lipids. The w/v of DHPC in the NMR sample is ~50-fold higher than the w/v of lipid in the liposome sample. Thus, the effective rimantadine concentration in the NMR sample is about 20-fold higher than that in the functional assay. We chose DHPC because among all detergents tested, it provided the quality of spectra that allowed us to measure NMR parameters accurately.

How significant is the lipid-facing pocket? We think that although the lipid-facing site probably does not play a significant role in adamantane inhibition, it may still be useful in developing new antiviral compounds because Asp44 is likely where protons exit from the channel (Pielak and Chou, 2010b), and rimantadine binding at the Asp44 position is known to affect the dynamics of the tryptophan gates (Schnell and Chou, 2008).

The structure of the open state of the chimeric channel may be substantially different from that of the closed state because the TROSY-HSQC spectra at pH 7.5 and 6.1 are significantly different (Figures 2A and 2E). But the spectra of the rimantadine-bound state at these two pH values are similar (Figures 2B and 2F), suggesting that the closed and the open states converge to the same inhibited state upon interaction with the drug. Comparing the structures of the drug-bound and -unbound states in Figure 4C revealed small but clear differences for the regions wherein the rimantadine binds. We believe that the free energy of the structural rearrangement from the uninhibited to the inhibited state comes mostly from hydrophobic interactions between the drug adamantane cage and Val27 and Ala30 of the protein. It is clear from Figure 4C, right panel, that in changing from the uninhibited to the inhibited state, Val27 and Ala30 methyl groups have reorganized to maximize VDW contacts with the adamantane cage. This reorganization involves both twisting and tighter packing of the TM helices.

Our NMR titration data in Figure 2 also show that although the chemical shifts of the drug-bound state at pH 7.5 and 6.1 are very similar, the peaks corresponding to the drug-bound population at pH 6.1 are ~5-fold weaker than those at pH 7.5 under twice as high rimantadine concentration (Figures 2B and 2F).

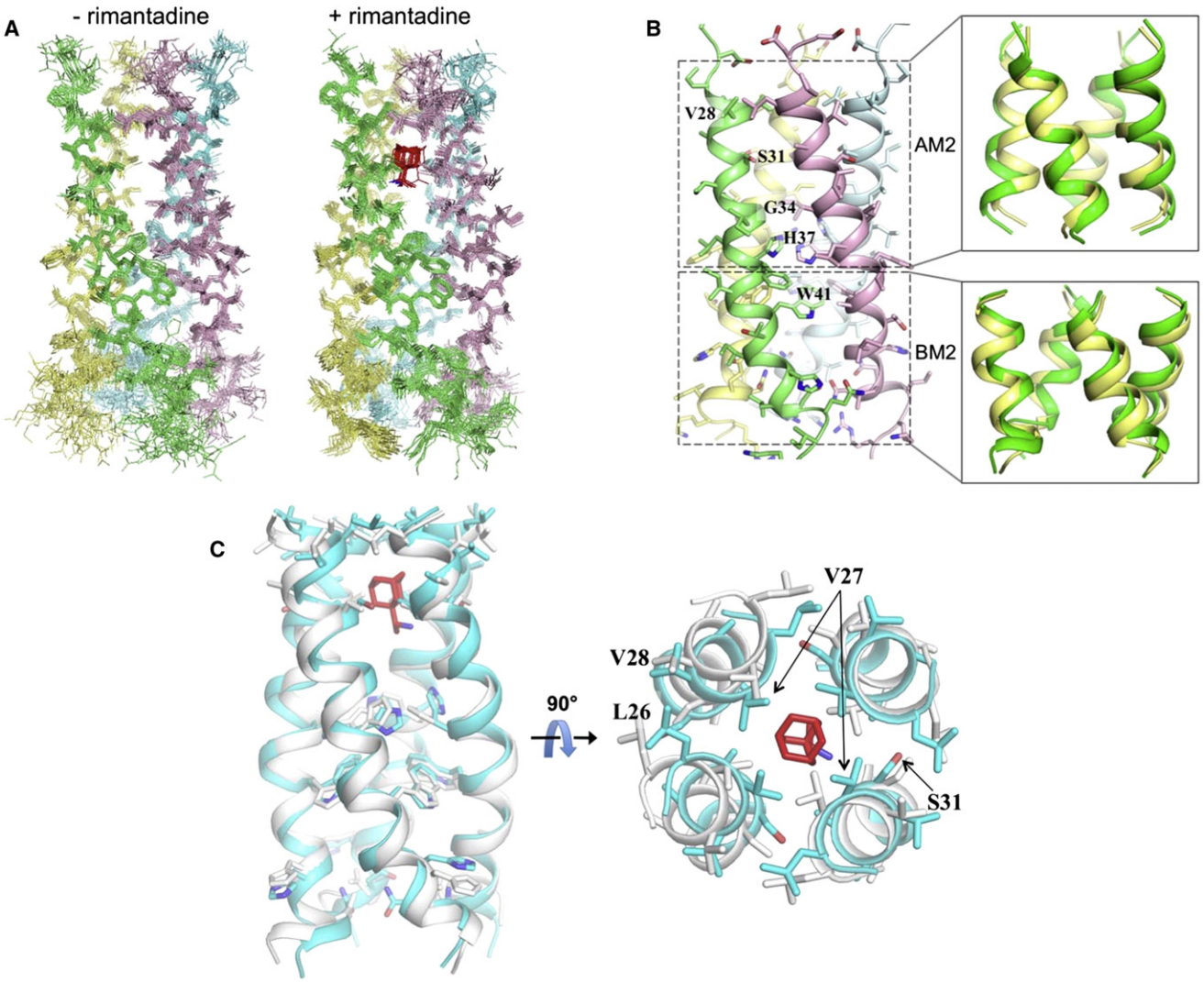


**Figure 4. Solution Structures of the $(AM2\text{-}BM2)_{TM}$ Channel in the Absence and Presence of Rimantadine**

(A) Ensembles of 15 low-energy structures of the drug-free (left) and drug-bound (right) chimera channels, determined at pH 7.5. Rimantadine is highlighted in red. (B) Ribbon representation of the drug-free $(AM2\text{-}BM2)_{TM}$ tetramer (left), and overlay of its AM2 and BM2 regions (green) with the corresponding regions (yellow) of the AM2 (PDB code: 2RLF) and BM2 (PDB code: 2KIX) structures (right). The backbone rmsds for the AM2 and BM2 regions are 1.3 and 2.2 Å, respectively. (C) Overlay of the drug-free (white) and the drug-bound (cyan) chimera structures, showing substantial differences in helical packing.

This observation suggests that rimantadine binds preferentially to the closed state of the channel. We speculate that the open state is more dynamic, and that the increased dynamics would require paying higher entropic cost for the drug to "lock" the channel in the closed conformation. Indeed, earlier solution NMR measurements of the native AM2 channel showed that lowering the pH from 7.5 to 6.5 broadened most of the NMR peaks corresponding to the TM helix, and that the resonance broadening was due to increased conformational exchange in the open state of the channel.

The solution structure of rimantadine binding to the chimeric channel is overall similar to the crystal structure of amantadine binding to the AM2 TM domain (Stouffer et al., 2008), but the properties of the internal pockets that accommodate the adamantyl cage are significantly different. In the solution structure this pocket is completely hydrophobic, constituted by methyl groups of valines and alanines (Figure 6A). In the crystal structure the pocket is slightly larger, formed by methyl groups of Val27 and Ala30 as well as hydroxyl groups of Ser31 (Figure 6B). Some of these differences may be attributed to the structural difference between amantadine and rimantadine and/or to the different helix-helix packing in the two structures.

Does the high-resolution structure of the drug-channel complex explain the known drug-resistance mutations? Mutations that have been reported to confer drug resistance include L26F, V27A, A30T, S31N, G34E, and L38F, among which the S31N and V27A account for the vast majority of resistant viruses. The internal hydrophobic pocket specific for the adamantane cage is composed of methyl groups of Val27 and Ala30, and therefore, either the V27A or A30T mutation will fundamentally change the physical or chemical properties of the pocket and, thus, resist rimantadine binding. For example the structure of

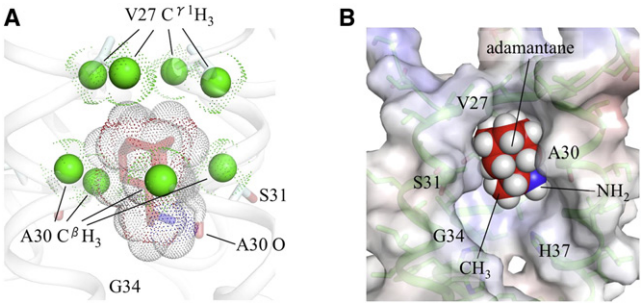


**Figure 5. Structural Details of Rimantadine Binding inside the Chimera Channel**

(A) Hydrophobic and polar interactions between rimantadine and protein. The eight methyl groups (four $C^{\gamma 1}H_3$ from Val27 and four $C^{\beta}H_3$ from Ala30) that are in VDW contacts with the adamantane cage of rimantadine are shown as green balls.

(B) Surface representation of the channel showing the internal hydrophobic pocket that wraps around the adamantane cage of rimantadine. One subunit of the tetramer was removed to unveil the channel interior.

the V27A mutant of AM2 (Pielak and Chou, 2010b) shows that replacing Val27 with Ala greatly decreases the hydrophobic surface of the internal pocket. Although the G34E mutation is unlikely to affect the pocket for the adamantane, addition of the large glutamic acid at this position will certainly cause steric collision with the amino and methyl groups of the drug (Figure 5A). Moreover, introducing four negative charges inside the small pore could alter the channel conformation.

Resistance conferred by the S31N mutation is less straightforward to explain because the Ser31 side chains face the helix-helix interface in both drug-bound and free chimeric channel and do not appear to be involved in any direct interactions with rimantadine. This structural result is consistent with earlier functional studies, which showed that introducing the S31A mutation in the AM2 channel has essentially no effect on rimantadine or amantadine inhibition (Pielak et al., 2009). A plausible explanation for resistance due to S31N is that replacing the relatively small serine with the bulkier asparagine at this position prevents the two adjacent TM helices from being close enough to form the inhibited structure (Figure 4C). Indeed, the solution NMR structure of the S31N mutant of AM2 showed that the Asn31 side chain is on average positioned at the helical-packing interface, like that of Ser31 in the wild-type AM2 channel (Pielak et al., 2009). Furthermore, chemical crosslinking data show that the S31N mutation leads to significantly weaker packing of the TM helices in the AM2 tetramer (Pielak et al., 2009). Therefore, it is likely that the bulkier Asn31 side chains in the helix-helix interface prevent the helices from forming the tight hydrophobic pocket seen in all structures. The L26F and L38F mutations have also been reported to confer partial resistance (Wang et al., 1993). According to the structure, Leu26 and Leu38 are also in the helical-packing interface; their replacements with phenylalanine could have a similar effect as that of the S31N mutation.

In conclusion, we have developed an NMR system for the channel domain of the AM2-BM2 chimera that supports rimantadine binding inside the channel and have shown that this system is relevant for structural characterization of the binding of the adamantane family antiviral compounds. The NMR data unambiguously define the structures of the drug-bound and -unbound forms of the channel. At pH 7.5 and in the absence of the drug, the AM2 portion of the chimera (residues 24–37) is structurally very similar to that of the wild-type AM2 channel determined under similar conditions. Rimantadine binds inside the pore near the N-terminal end of the channel. The spherically shaped adamantane forms VDW contacts with a cluster of methyl groups of Val27 and Ala30 from the four subunits. Consequently, drug binding causes tighter packing of the TM helices. In addition the drug amino group has a polar contact with the backbone carbonyl oxygen of Ala30 of one of the four subunits; this interaction may be important for defining the orientation of the drug molecule in the pore. The new structures imply that the known drug-resistance mutations may confer resistance by changing the hydrophobic property of the pore and/or by destabilizing the channel assembly to prevent the formation of the compact, drug-bound form of the channel. Finally, our results strongly support the model that the adamantane family compounds block the proton transport of the AM2 channel by binding inside the pore, while providing fine structural details to aid rational design of better adamantane derivatives for overcoming drug resistance.

## EXPERIMENTAL PROCEDURES

### Sample Preparation

The $(AM2\text{-}BM2)_{TM}$ peptide ($^{18}$RSNDSSDPLV$^{27}$VAASIIGIL$^{37}$HFIAWTIGHL $^{47}$NQIKR$^{52}$G) was cloned, expressed, and purified as previously described (Schnell and Chou, 2008). Briefly, the protein was expressed as a fusion to

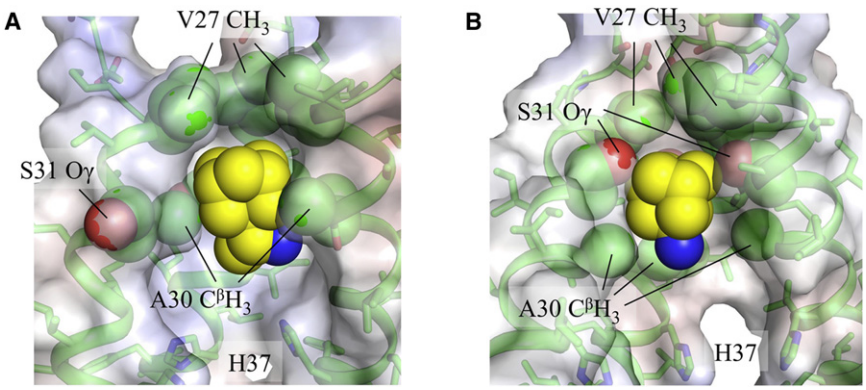


**Figure 6. Comparing the Solution and Crystal Structures of Drug Binding**

Combined surface, ribbon, and sphere representation of the pore-binding sites described by (A) the solution structure of rimantadine binding to the chimeric channel (PDB code: 2LJC), and (B) the crystal structure of amantadine binding to the TM domain of AM2 channel (PDB code: 3C9J). One subunit of the tetramer was removed to unveil the channel interior. Side chains of important residues such as Val27, Ala30, and Ser31 are shown as spheres.

His9-trpLE that formed inclusion bodies. The $(AM2\text{-}BM2)_{TM}$ peptide was released from the fusion protein by cyanogen bromide digestion in 70% formic acid. The digest was dialyzed against water to remove most of the formic acid, lyophilized, and redissolved in 2:1:2 hexafluoroisopropanol:formic acid:water. The peptide was separated on a C4 column (Grace-Vydac) by reverse-phase chromatography. The lyophilized peptide was then refolded by dissolving in 6 M guanidine and 150 mM DHPC and dialyzing against the final NMR buffer. NMR samples typically contained 1.2–1.8 mM $(AM2\text{-}BM2)_{TM}$ (monomer), 300 mM DHPC, and 40 mM sodium phosphate. Rimantadine was added to the concentrated NMR sample.

### Liposomal Proton Flux Assay

The exact protocol of the liposome assay used here for measuring proton conductance of the $(AM2\text{-}BM2)_{TM}$ channel was described in Pielak et al. (2009). Briefly, liposomes were made with identical pH and ion concentrations inside and outside, but highly buffered inside and only weakly buffered outside. Protein-mediated conductance of protons from the external bath into the liposome interior was initiated by adding hydrochloric acid under continuous rapid mixing. Proton flux was monitored as an increase in pH of the external bath. The final liposome sample was 1.5 ml and contained ~5 mg/ml lipid, 6 μM $(AM2\text{-}BM2)_{TM}$ peptide, and 0.1 μM valinomycin.

### NMR Spectroscopy

NMR experiments were conducted at 30°C on spectrometers equipped with cryogenic probes (Bruker, Billerica, MA). Data for the drug-bound and -unbound states were collected using samples at pH 7.5 with and without 50 mM rimantadine, respectively. Sequence-specific assignment of backbone $^{1}H^{N}$, $^{15}N$, and $^{13}C^{\alpha}$ chemical shifts was accomplished using triple-resonance experiments that were transverse relaxation optimized (tr), including three-dimensional (3D) tr-HNCA and tr-HNCOCA (Kay et al., 1990; Salzmann et al., 1999) recorded with a $^{15}N$-, $^{13}C$-, and 85% $^{2}H$-labeled protein. For assigning NOEs involving both backbone and side-chain protons, we prepared samples containing $^{15}N$-, $^{13}C$-labeled protein and deuterated DHPC (D22-DHPC) (Avanti Polar Lipids, Inc.), and used them to record 3D $^{15}N$-edited NOESY-tr-HSQC (110 ms NOE mixing), $^{13}C$-edited methyl NOESY (150 ms NOE mixing), and $^{13}C$-edited aromatic NOESY (150 ms NOE mixing). For identifying contacts between neighboring subunits, we prepared a mixed sample in which 50% of the monomers were perdeuterated and $^{15}N$-labeled protein and 50% protonated and $^{13}C$-labeled, and used it to record 3D $^{15}N$-edited NOESY-tr-HSQC (200 ms NOE mixing). This experiment allowed us to observe exclusively NOE cross-peaks between the $^{15}N$-attached exchangeable protons of one subunit and the $^{13}C$-attached protons of the neighboring subunits. For identifying intermolecular contacts between the protein and the drug, we prepared a sample containing 100% $^{15}N$-labeled and perdeuterated $(AM2\text{-}BM2)_{TM}$, 50 mM rimantadine, and deuterated DHPC, and used it to collect 3D $^{15}N$-edited NOESY-tr-HSQC (250 ms NOE mixing). Backbone $^{1}H\text{-}^{15}N$ RDCs were measured using a pair of $^{1}H\text{-}^{15}N$ HSQC and $^{1}H\text{-}^{15}N$ tr-HSQC spectra, recorded with $^{15}N$-, $^{13}C$-, and 85% $^{2}H$-labeled channels marginally oriented in 20 mg/ml DNA nanotubes (Douglas et al., 2007).

### Structure Determination

Structures of the drug-bound and -unbound chimera channels were calculated using the program Xplor-NIH (Schwieters et al., 2003). The monomer structures were first calculated from random coil using intrasubunit NOE-derived distance restraints, backbone dihedral restraints derived from chemical shifts using the TALOS program (Cornilescu et al., 1999), and RDC restraints. A total of ten monomer structures were calculated using a standard simulated annealing (SA) protocol in which the bath temperature was cooled from 1000 to 20 K. Four copies of the lowest-energy monomer structure calculated above were used to construct an initial model of the $(AM2\text{-}BM2)_{TM}$ tetramer. The assembled structure was then refined using the similar SA protocol in the presence of inter-subunit and protein-drug NOE restraints and all other intrasubunit restraints. For each experimental inter-subunit restraint between two adjacent subunits, four identical distance restraints were assigned respectively to all pairs of neighboring subunits to satisfy the condition of C4 rotational symmetry. For NOEs between the equivalent protons on the adamantyl cage and the peptide, distance restraints were applied to all subunits of the tetramer. For NOE between the rimantadine methyl group and the peptide, distance restraint was applied to any one of the four subunits. During the annealing run the bath was cooled from 1000 to 20 K. The NOE restraints were enforced by flat-well (uncertainty in distances) harmonic potentials, with the force constant ramped from 20 to 50 kcal $mol^{-1}$ $Å^{-2}$. The backbone dihedral angle restraints were also enforced by flat-well (±15°) harmonic potentials, with the force constant ramped from 100 to 300 kcal $mol^{-1}$ $rad^{-2}$. The RDC force constant was ramped from 0.01 to 1.0 kcal $mol^{-1}$ $Hz^{-2}$. In addition to experimental restraints, a weak database-derived "Rama" potential function (Kuszewski et al., 1997) was ramped from 0.02 to 0.2 (dimensionless force constant) for the general treatment of side-chain rotamers. Other force constants, commonly used in NMR structure calculation, were: k(vdw) = 0.02 → 4.0 kcal $mol^{-1}$ $Å^{-2}$, k(impr) = 0.1 → 1.0 kcal $mol^{-1}$ $degree^{-2}$, and k(bond angle) = 0.4 → 1.0 kcal $mol^{-1}$ $degree^{-2}$. For either drug-bound or -unbound state, a total of 75 tetramer structures were calculated, and 15 low-energy structures were selected as the structural ensemble. Ramachandran plot statistics for the chimera-rimantadine complex are as follows: most favored (97.0% for drug bound, 96.3% for unbound); additionally allowed (2.8% for drug bound, 3.2% for unbound); generously allowed (0.1% for drug bound, 0.5% for unbound); and disallowed (0.1% for drug bound, 0.1% unbound).

## ACCESSION NUMBERS

Coordinates and experimental restraints have been submitted to the Protein Data Bank with accession codes 2LJB for the chimeric channel without drug and 2LJC for the chimeric channel in complex with rimantadine.

## SUPPLEMENTAL INFORMATION

Supplemental Information includes four figures and can be found with this article online at doi:10.1016/j.str.2011.09.003.

## ACKNOWLEDGMENTS

The authors thank Stephen Harrison for critical reading of the manuscript and Gaëtan Bellot for help with DNA nanotube preparation. The work was supported by NIH Grants AI067438 and 1U54GM094608 (to J.J.C.).

Received: August 15, 2011
Revised: September 12, 2011
Accepted: September 12, 2011
Published: November 8, 2011

## REFERENCES

Andreas, L.B., Eddy, M.T., Pielak, R.M., Chou, J., and Griffin, R.G. (2010). Magic angle spinning NMR investigation of influenza A M2(18-60): support for an allosteric mechanism of inhibition. J. Am. Chem. Soc. *132*, 10958–10960.

Bright, R.A., Shay, D.K., Shu, B., Cox, N.J., and Klimov, A.I. (2006). Adamantane resistance among influenza A viruses isolated early during the 2005-2006 influenza season in the United States. JAMA *295*, 891–894.

Cady, S.D., and Hong, M. (2008). Amantadine-induced conformational and dynamical changes of the influenza M2 transmembrane proton channel. Proc. Natl. Acad. Sci. USA *105*, 1483–1488.

Cady, S.D., Schmidt-Rohr, K., Wang, J., Soto, C.S., Degrado, W.F., and Hong, M. (2010). Structure of the amantadine binding site of influenza M2 proton channels in lipid bilayers. Nature *463*, 689–692.

Cornilescu, G., Delaglio, F., and Bax, A. (1999). Protein backbone angle restraints from searching a database for chemical shift and sequence homology. J. Biomol. NMR *13*, 289–302.

Davies, W.L., Grunert, R.R., Haff, R.F., McGahen, J.W., Neumayer, E.M., Paulshock, M., Watts, J.C., Wood, T.R., Hermann, E.C., and Hoffmann, C.E. (1964). Antiviral Activity of 1-Adamantanamine (Amantadine). Science *144*, 862–863.

 

Douglas, S.M., Chou, J.J., and Shih, W.M. (2007). DNA-nanotube-induced alignment of membrane proteins for NMR structure determination. Proc. Natl. Acad. Sci. USA *104*, 6644–6648.

Hay, A.J., Wolstenholme, A.J., Skehel, J.J., and Smith, M.H. (1985). The molecular basis of the specific anti-influenza action of amantadine. EMBO J. *4*, 3021–3024.

Helenius, A. (1992). Unpacking the incoming influenza virus. Cell *69*, 577–578.

Jing, X., Ma, C., Ohigashi, Y., Oliveira, F.A., Jardetzky, T.S., Pinto, L.H., and Lamb, R.A. (2008). Functional studies indicate amantadine binds to the pore of the influenza A virus M2 proton-selective ion channel. Proc. Natl. Acad. Sci. USA *105*, 10967–10972.

Kay, L.E., Ikura, M., Tschudin, R., and Bax, A. (1990). Three-dimensional triple resonance NMR spectroscopy of isotopically enriched proteins. J. Magn. Reson. *89*, 496–514.

Khurana, E., Dal Peraro, M., DeVane, R., Vemparala, S., DeGrado, W.F., and Klein, M.L. (2009). Molecular dynamics calculations suggest a conduction mechanism for the M2 proton channel from influenza A virus. Proc. Natl. Acad. Sci. USA *106*, 1069–1074.

Kuszewski, J., Gronenborn, A.M., and Clore, G.M. (1997). Improvements and extensions in the conformational database potential for the refinement of NMR and X-ray structures of proteins and nucleic acids. J. Magn. Reson. *125*, 171–177.

Lamb, R.A., Zebedee, S.L., and Richardson, C.D. (1985). Influenza virus M2 protein is an integral membrane protein expressed on the infected-cell surface. Cell *40*, 627–633.

Mould, J.A., Paterson, R.G., Takeda, M., Ohigashi, Y., Venkataraman, P., Lamb, R.A., and Pinto, L.H. (2003). Influenza B virus BM2 protein has ion channel activity that conducts protons across membranes. Dev. Cell *5*, 175–184.

Ohigashi, Y., Ma, C., Jing, X., Balannick, V., Pinto, L.H., and Lamb, R.A. (2009). An amantadine-sensitive chimeric BM2 ion channel of influenza B virus has implications for the mechanism of drug inhibition. Proc. Natl. Acad. Sci. USA *106*, 18775–18779.

Oxenoid, K., and Chou, J.J. (2005). The structure of phospholamban pentamer reveals a channel-like architecture in membranes. Proc. Natl. Acad. Sci. USA *102*, 10870–10875.

Paterson, R.G., Takeda, M., Ohigashi, Y., Pinto, L.H., and Lamb, R.A. (2003). Influenza B virus BM2 protein is an oligomeric integral membrane protein expressed at the cell surface. Virology *306*, 7–17.

Pielak, R.M., and Chou, J.J. (2010a). Kinetic analysis of the M2 proton conduction of the influenza virus. J. Am. Chem. Soc. *132*, 17695–17697.

Pielak, R.M., and Chou, J.J. (2010b). Solution NMR structure of the V27A drug resistant mutant of influenza A M2 channel. Biochem. Biophys. Res. Commun. *401*, 58–63.

Pielak, R.M., Schnell, J.R., and Chou, J.J. (2009). Mechanism of drug inhibition and drug resistance of influenza A M2 channel. Proc. Natl. Acad. Sci. USA *106*, 7379–7384.

Pinto, L.H., Holsinger, L.J., and Lamb, R.A. (1992). Influenza virus M2 protein has ion channel activity. Cell *69*, 517–528.

Salzmann, M., Wider, G., Pervushin, K., and Wüthrich, K. (1999). Improved sensitivity and coherence selection for [15N,1H]-TROSY elements in triple resonance experiments. J. Biomol. NMR *15*, 181–184.

Schnell, J.R., and Chou, J.J. (2008). Structure and mechanism of the M2 proton channel of influenza A virus. Nature *451*, 591–595.

Schwieters, C.D., Kuszewski, J.J., Tjandra, N., and Clore, G.M. (2003). The Xplor-NIH NMR molecular structure determination package. J. Magn. Reson. *160*, 65–73.

Sharma, M., Yi, M., Dong, H., Qin, H., Peterson, E., Busath, D.D., Zhou, H.X., and Cross, T.A. (2010). Insight into the mechanism of the influenza A proton channel from a structure in a lipid bilayer. Science *330*, 509–512.

Stouffer, A.L., Acharya, R., Salom, D., Levine, A.S., Di Costanzo, L., Soto, C.S., Tereshko, V., Nanda, V., Stayrook, S., and DeGrado, W.F. (2008). Structural basis for the function and inhibition of an influenza virus proton channel. Nature *451*, 596–599.

Sugrue, R.J., and Hay, A.J. (1991). Structural characteristics of the M2 protein of influenza A viruses: evidence that it forms a tetrameric channel. Virology *180*, 617–624.

Tang, Y., Zaitseva, F., Lamb, R.A., and Pinto, L.H. (2002). The gate of the influenza virus M2 proton channel is formed by a single tryptophan residue. J. Biol. Chem. *277*, 39880–39886.

Wang, C., Takeuchi, K., Pinto, L.H., and Lamb, R.A. (1993). Ion channel activity of influenza A virus M2 protein: characterization of the amantadine block. J. Virol. *67*, 5585–5594.

Wang, C., Lamb, R.A., and Pinto, L.H. (1995). Activation of the M2 ion channel of influenza virus: a role for the transmembrane domain histidine residue. Biophys. J. *69*, 1363–1371.

Wang, J., Pielak, R.M., McClintock, M.A., and Chou, J.J. (2009). Solution structure and functional analysis of the influenza B proton channel. Nat. Struct. Mol. Biol. *16*, 1267–1271.

**Structure, *19***

# Supplemental Information

# Structural Investigation of Rimantadine Inhibition of the AM2-BM2 Chimera Channel of Influenza Viruses

**Rafal M. Pielak, Kirill Oxenoid, and James J. Chou**

**Inventory of Supplemental Information**

**Figure S1, related to Figure 2; it shows that in the sample used to record the spectra in Figure 2, the $(AM2\text{-}BM2)_{TM}$ peptide forms a homogeneous tetramer.**

**Figure S2, related to Figure 2; it shows that the $(AM2\text{-}BM2)_{TM}$ tetramers reconstituted in DHPC micelles and in DMPC/DHPC bicelles yielded very similar NMR spectra, indicating that the structures in detergent and in lipid bilayer are very similar.**

**Figure S3, related to Figure 2; it shows that the NMR resonances of the AM2-BM2 chimera in Figure 2A can be grouped into two subsets. The peaks that come from the AM2 sequence (18-36) are similar to the corresponding peaks from native AM2, and the same is true for those that come from the BM2 sequence (38-52). This analysis reveals partial structural similarities between the chimera and the native AM2 and BM2 channels.**

**Figure S4, related to Figure 2; it provides a quantitative description of the chemical shift differences between the drug-free (spectrum in Fig. 2A) and drug-bound (spectrum in Fig. 2B) states of the $(AM2\text{-}BM2)_{TM}$ channel.**

## Supplemental Information

# Structural investigation of rimantadine inhibition of the AM2-BM2 chimera channel of influenza viruses

**Rafal M. Pielak, Kirill Oxenoid, and James J. Chou**

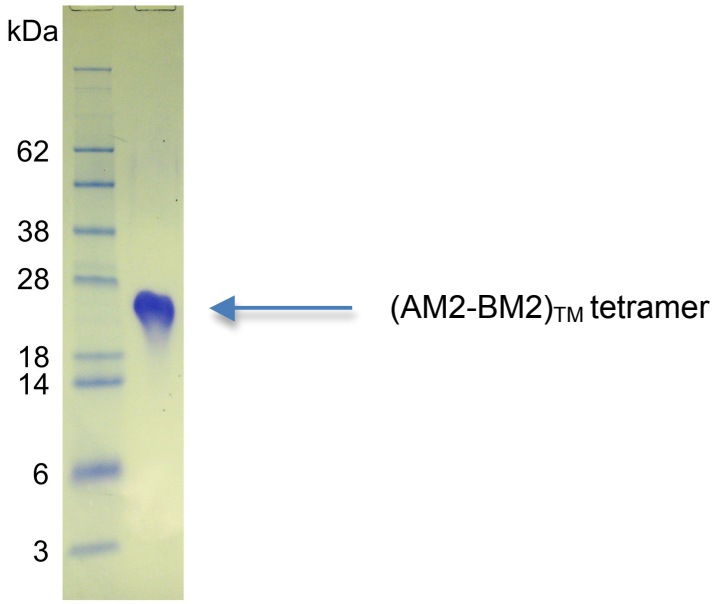


**Figure S1, related to Figure 2.** SDS-PAGE of a typical NMR sample of $(AM2\text{-}BM2)_{TM}$, for demonstrating the stability of the tetrameric assembly.

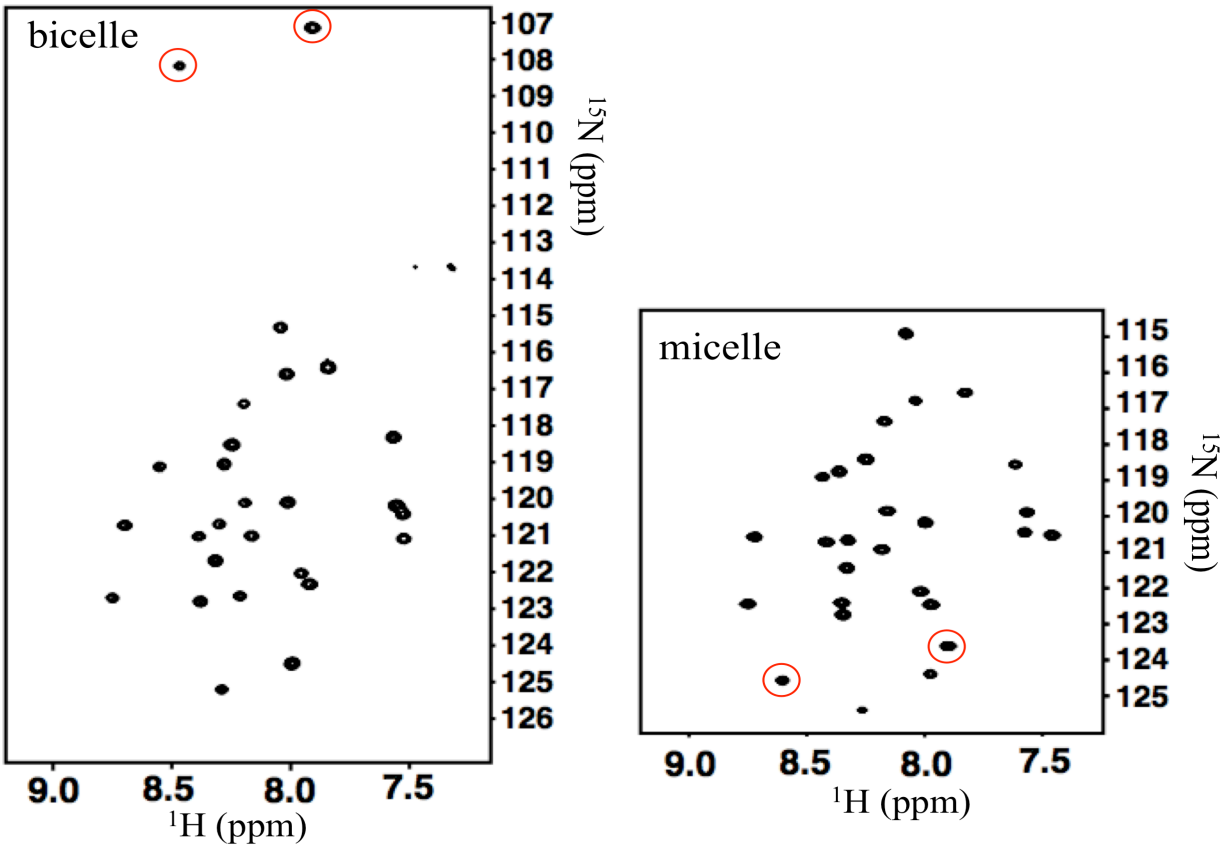


**Figure S2, related to Figure 2.** $^{1}$H-$^{15}$N TROSY-HSQC spectra of $(AM2\text{-}BM2)_{TM}$ reconstituted in DMPC/DHPC bicelles ($q$ = 0.3) (left) and DHPC micelles (right), recorded at 600 MHz $^{1}$H frequency and 30 °C. The peaks circled are glycine resonances that are folded in the micelle spectrum.

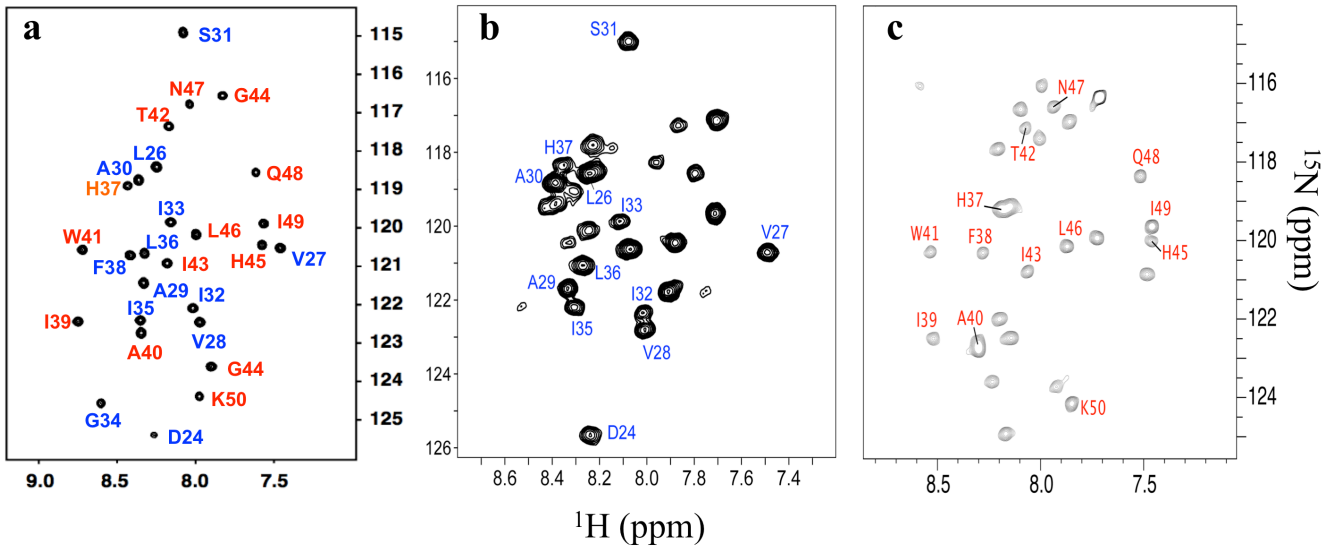


**Figure S3, related to Figure 2.** Comparison of $^{1}$H-$^{15}$N TROSY-HSQC spectra of (AM2-BM2)$_{TM}$ (**A**), AM2(18-60) (**B**), and BM2(1-33) (**C**), all reconstituted in DHPC micelles and at pH 7.5. The BM2 residue numbers in (C) are shifted such that the histidine in the channel has the same residue number as that in (AM2-BM2)$_{TM}$ and AM2(18-60).

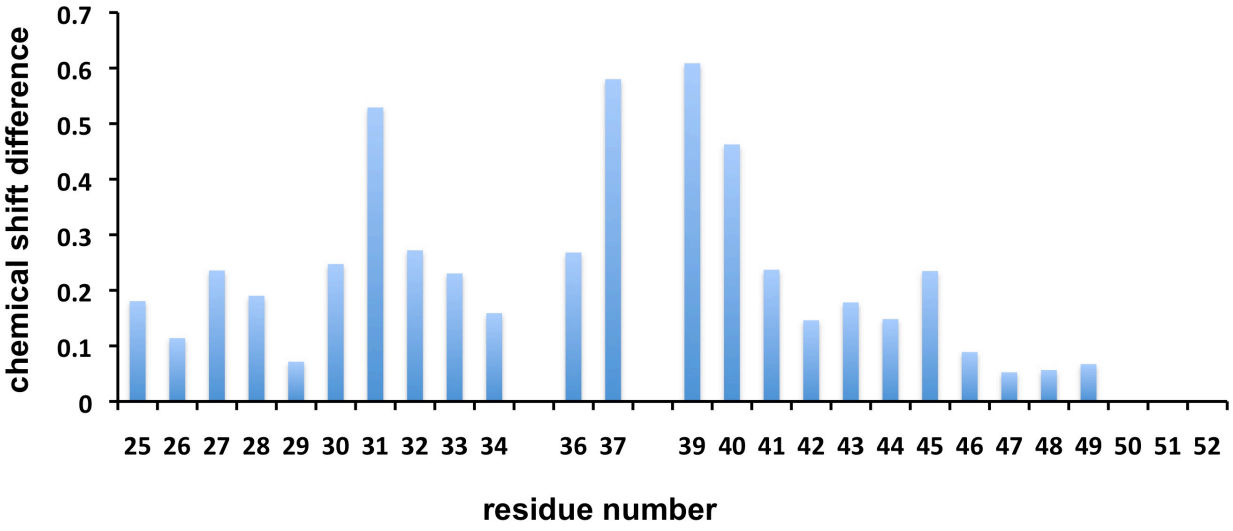


**Figure S4, related to Figure 2.** Chemical shift differences between the drug-free (spectrum in Fig. 2A) and drug-bound (spectrum in Fig. 2B) states of the $(AM2\text{-}BM2)_{TM}$ channel. The residue-specific chemical shift differences were quantified by the chemical shift distance, $\delta = \left[(\Delta H)^2 + (\Delta N/\eta)^2\right]^{1/2}$, where $\eta$ is the ratio of total resonance dispersion of $^{15}N$ to that of $^{1}H^{N}$ in ppm, and $\Delta H$ and $\Delta N$ are $^{1}H^{N}$ and $^{15}N$ chemical shift differences in ppm, respectively.